Space-charge driven origin of the reversible pyrocurrent peaks in $Cu_{1-x}Cd_xCr_2O_4$

Abhishek Das,[1] Riju Pal ,[2] Sakshi Mehta,[3] Kazi Parvez Islam ,[1] Abhishake Mondal ,[3]
Atindra Nath Pal ,[2] and Debraj Choudhury [1,*]

[1]*Department of Physics, Indian Institute of Technology Kharagpur, West Bengal 721302, India*
[2]*S. N. Bose National Center for Basic Sciences, Kolkata 700106, India*
[3]*Solid State and Structural Chemistry Unit, Indian Institute of Science Bengaluru, Karnataka 560012, India*

$CuCr_2O_4$, which belongs to the family of AB_2O_4 spinels, was recently reported to be a type-I multiferroic material. The observations of type-I multiferroicity, i.e., where ferroelectricity (FE) arises from a structural origin, is rare in the AB_2O_4 spinel family, thus this result is significant. The role of both Jahn-Teller (JT) active Cu^{2+} and Cr sublattice magnetic ordering was suggested in the earlier study, and a more careful investigation to elucidate the origin of the observed FE is required. With the aim to elucidate the origin of the observed FE, we carried out a detailed investigation of the structural, electrical, and magnetic properties of a $Cu_{1-x}Cd_xCr_2O_4$ ($0 \leqslant x \leqslant 1$) series, that enables an x-dependent controlled tuning of the Cu^{2+} driven structural and Cr-sublattice driven magnetic transition temperatures. We track and investigate the correlation of the observed pyrocurrent peaks with the temperature-dependent structural and magnetic transitions in this series for various x members. From careful investigations, we rule out any intrinsic origin and establish a space-charge or extrinsic origin for the observed switchable pyrocurrent peaks that point to an absence of ferroelectricity.

I. INTRODUCTION

Magnetoelectric multiferroic materials, which are simultaneously ferro(antiferro)magnetic and ferroelectric with a cross-coupling between the two order parameters are extremely promising as next generation spintronic materials [1–4]. Transition metal oxides crystallizing in the spinel crystal structure are well established to exhibit a strong coupling between their structural, magnetic, and orbital degrees of freedom [5–8]. Identification of novel multiferroic materials possessing a spinel structure have, thus, been actively pursued over the years [9–15]. Multiferroic materials can be broadly classified into two classes: Type-I and type-II multiferroic materials. In type-I multiferroic materials, ferroelectricity arises from the structural origin from the lack of inversion symmetry of the underlying crystalline lattice [16–19]. In type-II multiferroic materials, ferroelectricity arises due to the breaking of inversion symmetry by the emergent magnetic ordering [20–24]. While many type-II multiferroic materials have been realized in the spinel family [9–13], identifications of a type-I multiferroic spinel compound have mostly remained elusive with the exceptions of a few recent reports [14,15]. In this regard, a recent report of realization of type-I multiferroicity in a chromate spinel oxide, $CuCr_2O_4$, is particularly significant [25]. Ferroelectric order is reported in $CuCr_2O_4$ well above its magnetic ordering temperatures. The cubic spinel structure of $CuCr_2O_4$ is shown in Fig. 1(a), where the B-site Cr ions crystallize in a highly frustrated pyrochlore lattice [seen in Fig. 1(b)]. Driven by the orbitally active $Cu^{2+}(3d^9)$ ions

[while $Cr^{3+}(3d^3)$ is Jahn-Teller (JT) inactive], as shown in Figs. 1(c) and 1(d), $CuCr_2O_4$ undergoes a reduction in symmetry from cubic $Fd\bar{3}m$ to tetragonal $I4_1/amd$ (with $c < a$) at 853 K [26–28]. This cubic (C) to tetragonal ($T1$) structural transition in $CuCr_2O_4$ is then followed by a presumably spin-orbit coupling driven weak tetragonal ($T1$) to orthorhombic (O) structural transition [29–31] associated with the onset of long-range ferrimagnetic (FIM) ordering at 125 K [32,33]. Intriguingly, presence of the above structural transition at 125 K was recently ruled out and instead a higher temperature structural transition, from tetragonal $I4_1/amd$ to polar orthorhombic $Ima2$ at 170 K associated with the onset of ferroelectricity, has been pointed out [25]. Although the role of JT-active Cu^{2+} ions has been stressed to be important to lead to the structural transition into the polar phase at 170 K [25], the proposed scenario is intriguing given that Cu^{2+} electrons already lose their orbital degree of freedom at much higher temperatures ($\sim$853 K). Further, the role of the Cr-sublattice magnetic ordering of $CuCr_2O_4$, which is observed at much higher temperatures ($\sim$155 K) than the long-range FIM ordering at 125 K [34], has also been suggested [25] for the observed ferroelectricity. Such a sublattice magnetic ordering, as recently observed for $MnCr_2O_4$ [35], can indeed be associated with important structural modifications and become critical for the onset of ferroelectricity (FE). Any role of the Cr-sublattice magnetic ordering in the observed ferroelectricity of $CuCr_2O_4$, however, remains to be carefully investigated.

A larger (compared to Cu^{2+}) Cd^{2+}-ion doped $CuCr_2O_4$, namely $Cu_{1-x}Cd_xCr_2O_4$ series, was synthesized and characterized to shed light on the origin of the ferroelectricity in $CuCr_2O_4$. The dilution of magnetically and orbitally active $Cu^{2+}(3d^9)$ ions with nonmagnetic and orbitally inactive $Cd^{2+}(4d^{10})$ is expected to modulate the Cu^{2+} driven transi-

024104-1
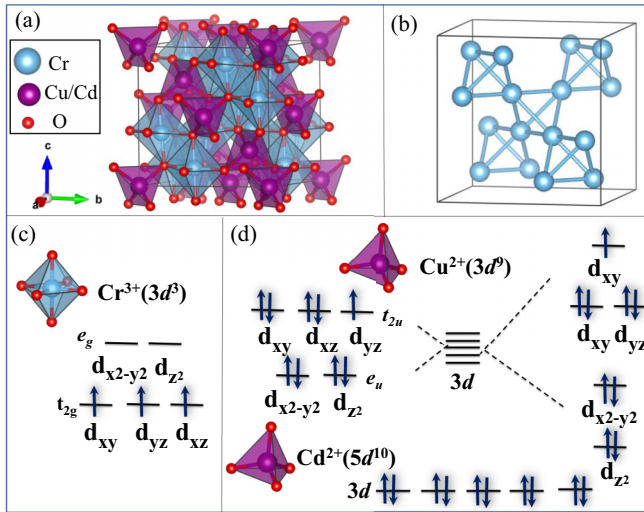
FIG. 1. (a) Cubic crystal structure of $CuCr_2O_4$ spinel, where Cu^{2+}/Cd^{2+} and Cr^{3+} ions are within tetrahedral and octahedral oxygen environments, respectively. (b) The pyrochlore network (corner shared tetrahedra) of the magnetic B-site ions. Schematic electronic configurations for the octahedrally coordinated (c) $Cr^{3+}(3d^3)$ and tetrahedrally coordinated (d) $Cu^{2+}(3d^9)$ and $Cd^{2+}(4d^{10})$ ions

tions and thereby elucidate any role of Cu^{2+} on the observed FE order in $CuCr_2O_4$. Also the larger Cd^{2+} (ionic radius $\sim$0.78 Å compared to 0.57 Å of Cu^{2+}) ions are expected to lead to an increase in the overall Cr-Cr distance, which will enable controlled modulation of the Cr-sublattice magnetic ordering temperature and bring out its role in the observed ferroelectric transition of $CuCr_2O_4$. Intriguingly, in agreement with the earlier results on $CuCr_2O_4$ [25], clear and switchable pyrocurrent peaks can be identified throughout the series at temperatures much above the corresponding long-range FIM ordering temperatures. Due to the expected structural tunings, as discussed earlier, the magnetic ordering temperatures progressively decrease with increased Cd doping. The temperatures of the Cu^{2+} JT-distortion driven structural transition also gets controllably tuned and lead to a rich magneto-structural phase diagram for the $Cu_{1-x}Cd_xCr_2O_4$ series. However, the temperatures at which the pyrocurrent peaks are observed in $Cu_{1-x}Cd_xCr_2O_4$ compounds were surprisingly found to remain nearly similar with Cd doping. Thus any role of JT-active Cu^{2+} and Cr-sublattice magnetic ordering on the observed pyrocurrent peaks can be conclusively ruled out. Further, temperature-dependent structural investigations also point towards absence of any structural transitions associated with the pyrocurrent peaks in this series. Finally, heating-rate-dependent and four-step pyrocurrent measurements (which are established to distinguish intrinsic ferroelectricity from extrinsic space-charge driven pyrocurrent signals), help to elucidate an extrinsic origin of the observed pyrocurrent peaks and thus to an absence of intrinsic FE in these samples.

II. METHODOLOGY

The well ground stoichiometric mixtures of Cr_2O_3, CuO, and CdO were sintered inside an evacuated quartz

tubes at 1150 °C for 24 h to synthesize polycrystalline $Cu_{1-x}Cd_xCr_2O_4$ samples. Temperature-dependent structural investigations on the synthesized samples were carried out using a laboratory x-ray diffraction (XRD) apparatus (with Cu-$K\alpha$) as well as synchrotron-based x-ray diffraction experiments ($\lambda = 0.8172$ Å) at the Indus2 beamline, Indore, India. Trace quantities of Cr_2O_3 impurity phase ($\sim$1 %) were detected from the XRD spectra. Structural parameters were determined from Rietveld refinement of the XRD data using the FULLPROF package [36]. Chemical homogeneity of the samples was investigated by employing energy dispersive x-ray (EDX) analyses. Scanning electron microscopy (SEM) images of the samples were collected in a secondary electron mode using the MERLIN apparatus. Temperature-dependent dielectric and pyrocurrent measurements were carried out using a Keysight E4990A impedance analyzer and a Keithley 6517B electrometer, respectively. For typical pyrocurrent measurements, each sample was first cooled to a temperature below the transition from a higher temperature under the presence of an applied electric field. To get rid of any surface charge effect, electrodes were then kept shorted for 2 hours. The sample was then heated to a higher temperature with various (fixed) heating rates while the temperature-dependent pyroelectric current was recorded. Further, to investigate the presence of any extrinsic contribution in the pyrocurrent signal, we carried out four-segment thermal cycling pyroelectric measurements by adapting the following steps [37–39]. Step 1: After poling the sample to a lower temperature and shorting the electrodes for 2 h, heat the sample to a temperature (T_W) just below the transition temperature. Step 2: Wait for 1 h at T_W. Step 3: Cool the sample to the lowest temperature. Step 4: Heat the sample again to the higher temperature above the transition. Temperature-dependent magnetization measurements were performed by a superconducting quantum interference device (SQUID) magnetometer from Quantum Design. Differential scanning calorimetric (DSC) measurements were also performed both in heating and cooling cycles to investigate the phase transition temperatures.

III. RESULTS AND DISCUSSIONS

Room-temperature XRD spectra and refined lattice parameters of $Cu_{1-x}Cd_xCr_2O_4$, as shown in Fig. 2(a), the inset of Fig. 2(b), and Fig. S1 of the Supplemental Material [40], clearly elucidate an x-dependent structural phase transition from tetragonal ($T1$) for $x < 0.6$ to cubic (C) for $x \geqslant 0.6$. In agreement with earlier reports on $CuCr_2O_4$ [26–28], the tetragonal $I4_1/amd$ space group (with $c < a$) was found to account well for the room-temperature structure of compositions with $x < 0.6$ and similarly cubic $Fd\overline{3}m$ space group was found adequate for $x \geqslant 0.6$. Rietveld refinements (refined parameters of all the samples are depicted in Table S1 of [40]) of the representative samples, $x = 0.2$ and $x = 0.8$, are shown in Fig. 2(b) and Fig. S2 of [40], respectively. Notably, the increase in average Cr-Cr distance with x, as shown in Fig. 2(c), is consistence with the larger size of the doped Cd^{2+} ion (ionic radii $\sim$0.78 Å) in place of the smaller Cu^{2+} ion (ionic radius $\sim$0.57 Å) in the $Cu_{1-x}Cd_xCr_2O_4$ series. EDX analyses reveal the presence of $\sim$5% Cu deficiency, likely arising from unintentional weighing of less Cu due to the hygroscopic nature
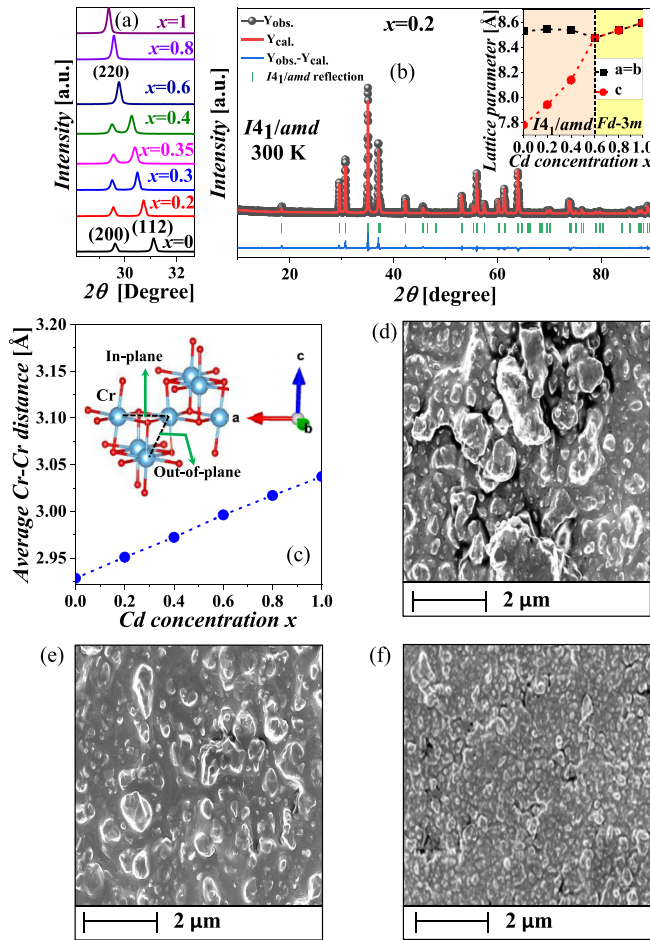
FIG. 2. (a) (200) and (112) tetragonal Bragg peaks, observable up to $x < 0.6$, merge into a single cubic Bragg peak (220) from $x = 0.6$. (b) Rietveld refinement of the XRD spectrum of $x = 0.2$ considering the $I4_1/amd$ space group. The inset of (b) highlights the variations of lattice parameters with x. (c) Variation of average Cr-Cr distance with x. The inset of (c) shows a pair of corner-shared CrO$_4$ tetrahedra in the tetragonal $I4_1/amd$ phase with two different (in-plane and out-of-plane) Cr-Cr distances. SEM images of (d) $x = 0$, (e) $x = 0.2$ and (f) $x = 0.6$.

of CuO, as shown in Table S2 of [40]. The microstructures of the samples, investigated using SEM, as shown in Figs. 2(d) and 2(f), suggest a more dominant role of the grain-boundary regions with increasing x in the series. Analyses of the associated dielectric relaxations [41–44] (included in Sec VI, Figs. S3 and S4, and Table S3 of [40]), which also include the contributions from grain and grain-boundary regions, indicate a similar trend.

In order to examine the role of the structural modifications in Cu$_{1-x}$Cd$_x$Cr$_2$O$_4$ on the tuning of the reported ferroelectricity in CuCr$_2$O$_4$, temperature-dependent pyrocurrent measurements were performed. The obtained results are shown in Figs. 3(a)–3(e). In agreement with the earlier results [25], a clear pyroelectric transition is observed at 175 K for $x = 0$ (CuCr$_2$O$_4$), as shown in Fig. 3(a). In addition, two more pyrocurrent peaks are observed at 60 and 140 K for $x = 0$. The reversible nature of all the pyro peaks seems to suggest the presence of ferroelectric order in CuCr$_2$O$_4$.
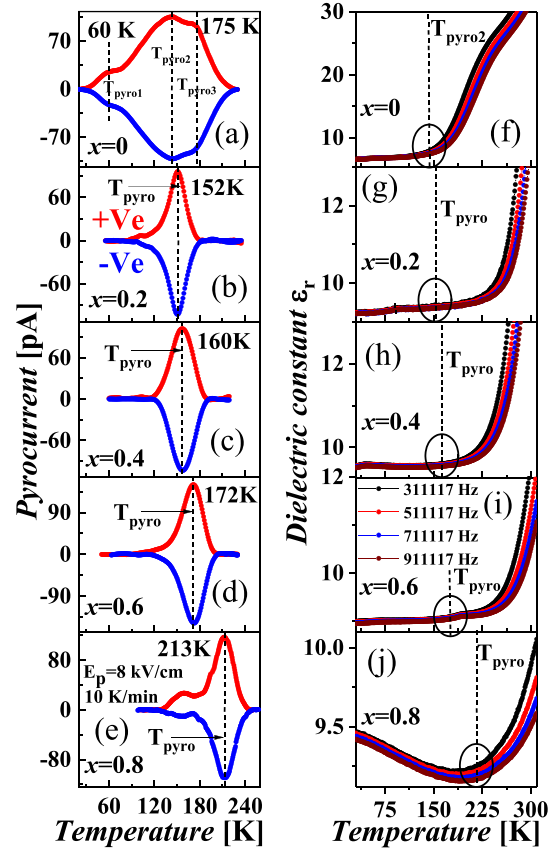
FIG. 3. Temperature-dependent pyrocurrent data, measured with 10 K/min heating rate for (a) $x = 0$, (b) $x = 0.2$, (c) $x = 0.4$, (d) $x = 0.6$, and (e) $x = 0.8$. Each sample was poled with poling voltage of $E_P = \pm 8$ kV/cm. [(f)–(j)] Highlighted temperature-dependent dielectric data for different x.

Interestingly, intense broad pyrocurrent peaks [which are reversible with opposite poling field, as shown in Figs. 3(b)–3(e)] are also observed at 152, 160, 172, and 213 K for $x = 0.2$, 0.4, 0.6, and 0.8 samples, respectively. Surprisingly, the corresponding transitions are not observable in the temperature dependence of the dielectric constant data for all the compositions, as shown in Figs. 3(f)–3(j). Instead, the dielectric constant values are found to rapidly rise just above T_{pyro}, the temperatures at which the pyrocurrent peaks are observed. The compound with $x = 1$ (CdCr$_2$O$_4$) is reported to have a zero magnetic field paraelectric state [45], which is also in agreement with our results. The absence of any clear pyroelectric peak for $x = 1$, around the temperatures in which they are observed for other x members, is also noted from Fig. S5 of [40].

In order to investigate the origin of the observed pyrocurrent peaks and their correlation with any magnetic ordering, temperature-dependent dc and ac magnetic measurements were carried out. We note that $x = 0$ (CuCr$_2$O$_4$) exhibits paramagnetic (PM) to FIM ordering (shown by a green arrow) at $T_{C1} = 125$ K [seen in Fig. 4(a)] and a weak Cr-sublattice ordering at $T_{C2} = 155$ K [later detected clearly through ac susceptibility data, as shown in Fig. 4(b)], consistent with earlier reports [32–34]. Progressive doping by nonmagnetic
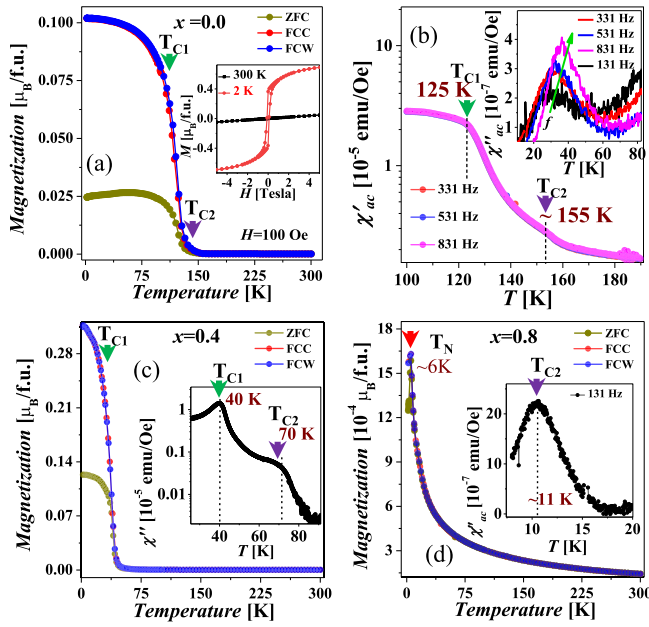
FIG. 4. Temperature dependence of dc magnetization (M) of (a) $x = 0$, (c) $x = 0.4$, and (d) $x = 0.8$, obtained after zero-field cooling (ZFC), field-cooled cooling (FCC), and field-cooled warming (FCW) with an applied magnetic field (H) of 100 Oe. (b) Real part (χ') of the ac susceptibility data of $x = 0$. The inset of (b) highlights the low temperature weak glassy magnetic ordering detected from the imaginary part (χ'') of the the ac susceptibility. The plot in the inset of (a) shows the isothermal M-H curves of $x = 0$ at 2 and 300 K, indicating its FIM character. The ac susceptibility data of $x = 0.4$ and 0.8 highlighting the Cr-sublattice ordering above FIM ordering are shown in the insets of (c) and (d), respectively. Green, red, and violet arrows indicate FIM ordering, AFM ordering, and Cr-sublattice ordering, respectively.

FIG. 5. (a) Continuous broadening of the (220) tetragonal peak below FIM ordering temperature at 125 K for $x = 0$, observed from normal XRD data. (b) The coincident (105) and (440) tetragonal reflections split below 125 K for $x = 0$, observed from synchrotron XRD data. The inset highlights the broadening of the (103) peak below 125 K. (c) The (220) tetragonal peak broadens below FIM ordering temperature at 90 K for $x = 0.2$. The same for the (512) peak is shown in the inset. (d) The (664) cubic reflection broadens below AFM ordering temperature at 6 K for $x = 0.8$. The same for the (620) peak is shown in the inset.

$Cd^{2+}(4d^{10})$ in place of magnetic A-site $Cu^{2+}(3d^9)$ ions and also an increase in the Cr-Cr distance with x [as seen in Fig. 2(c)] lead to a systematic tuning (reduction) of both T_{C1} and T_{C2} with increasing x, as shown in Figs. 4(a)–4(d) and also in Figs. S6 and S7 of [40]. Evolution from FIM (for $x < 0.8$) to essentially Cr-driven AFM order with a sudden drop in magnetization for $x \geqslant 0.8$ is evident from Fig. 4 and Fig. S6 of [40]. Also, from the field dependence of magnetization, shown in the inset to Fig. 4(a) and Fig. S8 of [40], we note that while $x = 0$ exhibits soft FIM-like behavior (i.e., saturated magnetization with small hysteresis loop), M-H loop gets more pronounced with increasing x up to $x = 0.4$ (possibly driven by disorder effects), beyond which it starts to shrink and becomes almost linear like an antiferromagnet at $x = 0.8$. An additional glassy magnetic ordering in $CuCr_2O_4$ (not observable for higher x members) at around 25 K, as shown in the inset of Fig. 4(b), is also observed. Importantly, we note that while the Cr-sublattice magnetic ordering temperature (T_{C2}) continues to decrease with increasing x, T_{C2} is discernible till $x = 0.8$ and not observable for $x = 1$ (as seen in the ac susceptibility data of $x = 1$ in the inset of Fig. S6(c) of [40]). This, however, is in marked contrast with the evolution of the pyrocurrent peak temperature, which continues to vary gradually up to $x = 0.8$ [see Figs. 3(a)–3(e)]. The

obtained magnetization results thus clearly rule out any role of the magnetic orderings behind the commencement of such pyrocurrent peaks in the $Cu_{1-x}Cd_xCr_2O_4$ series.

To investigate the role of a temperature-dependent structural transition in the observed pyrocurrent peaks, temperature-dependent normal as well as synchrotron-based XRD investigations were performed. For $x = 0$ ($CuCr_2O_4$), while XRD spectra between 300 and 150 K overlap, a clear broadening (opposite to the thermal broadening) of the (220) tetragonal peak was observed between 150 and 100 K from normal XRD data, as shown in Fig. 5(a), suggesting the onset of structural modifications only below 150 K. Our observation is consistent with the reported tetragonal ($T1$) to orthorhombic (O) structural phase transition at the FIM ordering temperature of 125 K [29–31]. Importantly, no such XRD spectral broadenings are noticeable across 175 K, i.e., around the temperature at which the pyrocurrent peak is observed for $x = 0$. The appearance of a structural transition at T_{C1} is also well supported by the temperature-dependent synchrotron XRD data, where coincident (105) and (440) reflections at 300 K are found to get split at 100 K, i.e., below the FIM ordering temperature of 125 K [30]. These structural results are, thus, notably not consistent with the claim of a tetragonal ($T1$) to polar orthorhombic
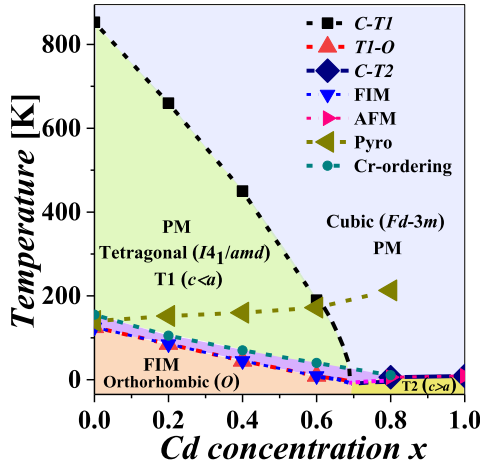
FIG. 6. Obtained magnetic and structural phase diagram of $Cu_{1-x}Cd_xCr_2O_4$.

($Ima2$) structural transition at 175 K associated with the pyrocurrent peak. Also, Rietveld refinements of the low temperature (at $T = 25$ K) XRD spectrum (refined spectra are shown in Figs. S9(a) and S9(c) of [40]) with the $Ima2$ space group did not yield a satisfactory fit as compared to the reported $Fddd$ space group (quantitatively in terms of better fitting parameters and also qualitatively since it reproduces the experimental XRD peak shapes better), as illustrated in Figs. S9(b) and S9(d) of [40]. Thus, the obtained structural results elucidate that $CuCr_2O_4$ undergoes a tetragonal $I4_1/amd$ ($c < a$) to orthorhombic $Fddd$ structural transition at the FIM ordering temperature at 125 K (instead of $Ima2$ at 175 K). A similar $T1$-O transition is illustrated by the broadening of the (220) peak below 90 K (FIM ordering temperature) for $x = 0.2$, as shown in the Fig. 5(c). The cubic (C) to tetragonal ($T1$) structural transition is driven by the Jahn-Teller active $Cu^{2+}(3d^9)$ ions, whereas the $T1$ to orthorhombic (O) structural transition at T_{C1} is presumably driven by the spin-orbit coupling. With increasing $Cd^{2+}(4d^{10})$ doping for $Cu^{2+}(3d^9)$ ions, the dilution of JT active Cu^{2+} ionic content leads to systematic reduction in the C-$T1$ structural transition temperature, as probed through temperature-dependent DSC data (Fig. S10 of [40]). The $T1$-O transition, which accompanies the FIM transition at T_{C1}, is also observed to reduce with increasing x (as shown in Fig. 5(c) and Figs. S11(a) and S11(b) of [40]). With significant dilution of the JT active Cu^{2+} ions, i.e., in the range $0.6 < x < 0.8$, the cubic to tetragonal structural transition merges with the long-range AFM transition at T_N, as shown in Fig. 5(d) and Fig. S11(c) for $x = 0.8$ and 1, respectively. Beyond this x composition, the nature of the tetragonal phase change to $T2$ (with $c > a$) [46,47]. A rich magnetostructural phase diagram, as shown in Fig. 6, is thus realized. Importantly, no structural phase transition is observed to arise concomitant or even around the pyrocurrent peak temperatures in any of the x compositions, as illustrated in Fig. 6. The temperatures associated with different transitions and corresponding magnetization values are listed in Table S4 of the Supplemental Material [40]. Notably, $Cu_{1-x}Co_xCr_2O_4$ [25] exhibits a very different magneto-structural phase diagram than $Cu_{1-x}Cd_xCr_2O_4$. Interestingly, both Cd^{2+} and Co^{2+} are JT-inactive ions; however, while the Cd^{2+} ion is

diamagnetic, Co^{2+} possesses a larger magnetic moment than the Cu^{2+} ion. The dilution of the A-site magnetic moment in $Cu_{1-x}Cd_xCr_2O_4$ against its strengthening in $Cu_{1-x}Co_xCr_2O_4$ is expected to lead to varying magnetic and spin-frustration induced structural properties [48]. Further, Cd^{2+} (ionic radius 0.78 Å) is a much larger ion than Cu^{2+} (ionic radius 0.57 Å), whereas the Co^{2+} ion (ionic radius 0.58 Å) is similar in size to the Cu^{2+} ion, which is also expected to lead to differences in strain-energy driven physical properties between the two series.

The absence of any magnetic, dielectric, and structural phase transitions associated with the pyrocurrent peaks for all x suggests a possible extrinsic origin for the observed pyrocurrent peaks in the $Cu_{1-x}Cd_xCr_2O_4$ series. Besides, the role of microstructures of the polycrystalline samples (as discussed earlier), i.e., the difference in conductivities between the grain and the grain-boundary regions (or at the sample-electrode interfaces) can lead to charge-carrier trapping at low temperatures. Subsequent raising of temperature of the sample can then lead to charge detrapping and to the presence of pyrocurrent peaks arising from microstructure effects. The presence of various kinds of defects, such as oxygen vacancies, can also lead to formation of defect dipoles. Temperature induced charge detrapping and conduction between defect dipole pairs are some notable extrinsic factors that can lead to pyrocurrent peaks [37,38,49–51]. To investigate such a scenario, four-segment thermal cycling pyroelectric measurements [37,38] and heating-rate-dependent pyrocurrent measurements were performed. The protocol for the former was discussed earlier. For $x = 0$ ($CuCr_2O_4$), three different wait temperatures T_W, i.e., below each of the pyrocurrent peak temperatures, were employed. In regards to the pyrocurrent peaks during cycle 4 of the four-segment check measurement, only two pyrocurrent peaks were observed, at completely different temperatures than those obtained without wait [as shown in Fig. 3(a) and also Fig. 7(b)]. This is in sharp contrast to the scenario of an intrinsic ferroelectric transition, in which case the pyrocurrent peak positions do not change even in cycle 4 [37,38], unlike the case for $x = 0$ [as shown in Figs. 7(a) and 7(b)]. The four-segment pyrocurrent measurements also elucidate an extrinsic origin of the pyrocurrent peaks for the doped compounds, as seen in Figs. 7(c) and 7(d) for $x = 0.4$ and Fig. S12 of [40] for other x members. Also, consistent with an extrinsic origin for the pyrocurrent peaks, the temperatures of the pyrocurrent peaks were found to increase on increasing the heating rate during measurement for all x compositions (the change was difficult to perceive for $x = 0$ given the broadness of the corresponding pyrocurrent peaks), as shown in Fig. S13 of [40]. The sharp increase in dielectric constant just above the pyrocurrent peak, as seen in Figs. 3(f)–3(j) and discussed earlier, also provides a vital clue to the likely space-charge origin for the later. Free charge carriers, which seem to get delocalized around T_{pyro}, thus seem to be the reason behind the appearance of such broad and intense pyrocurrent peaks in the investigated series.

IV. CONCLUSIONS

In conclusion, detailed magnetic and structural investigations have been carried out on the $Cu_{1-x}Cd_xCr_2O_4$ series
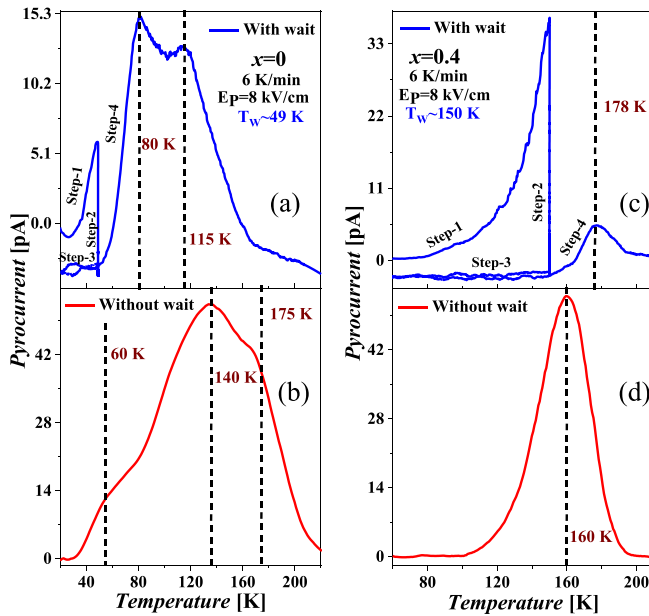
FIG. 7. The temperature-dependent pyrocurrent data of $x = 0$ (a) with wait (during four-segment thermal cyclic pyroelectric measurement) and (b) without wait. Pyrocurrent data of $x = 0.4$ (c) with wait (during four-segment thermal cyclic pyroelectric measurement) and (d) without wait. Measurements were done with 6 K/min heating rate and a poling voltage of 8 kV/cm. T_W is the waiting temperature during cycle 2.

to probe the origin of the observed ferroelectric order in $CuCr_2O_4$ at 170 K. Our study clearly elucidates that $CuCr_2O_4$ does not show any spontaneous ferroelectric order within the measured temperature range, although three distinct and reversible pyrocurrent peaks were observed through temperature-dependent pyrocurrent measurements. While a transition from FIM ordering to a dominant AFM ordering occurs beyond $x = 0.6$, a high temperature pyrocurrent peak continues to be observed up to $x = 0.8$. Our temperature-dependent structural and magnetization investigations rule out any correlation between observed pyrocurrent peaks with any structural or magnetic transitions in the whole series. Finally, through four-segment thermal cycling pyroelectric measurements, we have illustrated the extrinsic nature of the observed broad and intense pyrocurrent peaks, which likely arise from free charge carrier detrapping at the high temperature rather than spontaneous dipole moments.

ACKNOWLEDGMENTS

[1] M. Fiebig, T. Lottermoser, D. Meier, and M. Trassin, The evolution of multiferroics, Nat. Rev. Mater. **1**, 16046 (2016).

[2] N. A. Spaldin, and R. Ramesh, Advances in magnetoelectric multiferroics, Nat. Mater. **18**, 203 (2019).

[3] W. Eerenstein, N. D. Mathur, and J. F. Scott, Multiferroic and magnetoelectric materials, Nat. Mater. **442**, 759 (2006).

[4] S.-W. Cheong, and M. Mostovoy, Multiferroics: A magnetic twist for ferroelectricity, Nat. Mater. **6**, 13 (2007).

[5] S. Ji, S.-H. Lee, C. Broholm, T. Y. Koo, W. Ratcliff, S.-W. Cheong, and P. Zschack, Spin-lattice order in frustrated $ZnCr_2O_4$, Phys. Rev. Lett. **103**, 037201 (2009).

[6] V. Tsurkan, S. Zherlitsyn, S. Yasin, V. Felea, Y. Skourski, J. Deisenhofer, H.-A. Krug von Nidda, J. Wosnitza, and A. Loidl, Unconventional magnetostructural transition in $CoCr_2O_4$ at high magnetic fields, Phys. Rev. Lett. **110**, 115502 (2013).

[7] A. Rahaman, M. Chakraborty, T. Paramanik, R. K. Maurya, S. Mahana, R. Bindu, D. Topwal, P. Mahadevan, and D. Choudhury, Tetramer orbital ordering and lattice chirality in $MnTi_2O_4$, Phys. Rev. B **100**, 115162 (2019).

[8] Y. Nii, N. Abe, and T.-H. Arima, Orbital-spin-coupled fluctuations in spinel vanadate MnV_2O_4, Phys. Rev. B **87**, 085111 (2013).

[9] L. Zhao, L. Muzica, U. Schwarz, and A. C. Komarek, Multiferroicity in the frustrated spinel cuprate $GeCu_2O_4$, Phys. Rev. Mat. **2**, 041402(R) (2018).

[10] Y. Yamasaki, S. Miyasaka, Y. Kaneko, J.-P. He, T. Arima, and Y. Tokura, Magnetic reversal of the ferroelectric polarization in a multiferroic spinel oxide, Phys. Rev. Lett. **96**, 207204 (2006).

[11] K. Singh, A. Maignan, C. Simon, and C. Martin, $FeCr_2O_4$ and $CoCr_2O_4$ spinels: Multiferroicity in the collinear magnetic state? Appl. Phys. Lett. **99**, 172903 (2011).

[12] N. Ikeda, H. Ohsumi, K. Ohwada, K. Ishii, T. Inami, K. Kakurai, Y. Murakami, K. Yoshii, S. Mori, Y. Horibe and H. Kito, Ferroelectricity from iron valence ordering in the charge-frustrated system $LuFe_2O_4$, Nat. Mater. **436**, 1136 (2005).

[13] K. Dey, S. Majumdar, and S. Giri, Ferroelectricity in spiral short-range-ordered magnetic state of spinel $MnCr_2O_4$: Significance of topological frustration and magnetoelastic coupling, Phys. Rev. B **90**, 184424 (2014).

[14] J. K. Dey, A. Chatterjee, A.-C. Dippel, O. Gutowski, M. V. Zimmermann, S. Majumdar, and S. Giri, Rhombohedral distortion-driven ferroelectric order and exchange bias effect in geometrically frustrated $ZnFe_2O_4$, Phys. Rev. Mat. **5**, 014410 (2021).

[15] A. A. Bush, V. Ya. Shkuratov, K. E. Kamentsev, A. S. Prokhorov, E. S. Zhukova, B. P. Gorshunov, and V. I. Torgashev, Ferroelectricity in spinel solid solution $CoCr_2O_4$, Phys. Rev. B **85**, 214112 (2012).

[16] J. Wang, J. B. Neaton, H. Zheng, V. Nagarajan, S. B. Ogale, B. Liu, D. Viehland, V. Vaithyanathan, D. G. Schlom, U. V. Waghmare, N. A. Spaldin, K. M. Rabe, M. Wuttig, and R. Ramesh, Epitaxial $BiFeO_3$ multiferroic thin film heterostructures, Science **299**, 1719 (2003).

[17] B. B. Van Aken, T. T. M. Palstra, A. Filippetti, and N. A. Spaldin, The Origin of Ferroelectricity in Magnetoelectric $YMnO_3$, Nat. Mater. **3**, 164 (2004).

[18] W. Wang, J. Zhao, W. Wang, Z. Gai, N. Balke, M. Chi, H. N. Lee, W. Tian, L. Zhu, X. Cheng, D. J. Keavney, J. Yi, T. Z. Ward, P. C. Snijders, H. M. Christen, W. Wu, J. Shen, and X. Xu, Room-temperature multiferroic hexagonal LuFeO$_3$ films, Phys. Rev. Lett. **110**, 237601 (2013).

[19] P. Pal, K. Rudrapal, S. Mahana, S. Yadav, T. Paramanik, S. Mishra, K. Singh, G. Sheet, D. Topwal, A. R. Chaudhuri, and D. Choudhury, Origin and tuning of room-temperature multiferroicity in Fe-doped BaTiO$_3$, Phys. Rev. B **101**, 064409 (2020).

[20] N. Terada, D. D. Khalyavin, P. Manuel, F. Orlandi, C. J. Ridley, C. L. Bull, R. Ono, I. Solovyev, T. Naka, D. Prabhakaran, and A. T. Boothroyd, Room-temperature type-II multiferroic phase induced by pressure in cupric oxide, Phys. Rev. Lett. **129**, 217601 (2022).

[21] R. E. Newnham, J. J. Kramer, W. A. Schulze, and L. E. Cross, Magnetoferroelectricity in Cr$_2$BeO$_4$, J. Appl. Phys. **49**, 6088 (1978).

[22] T. Kimura, T. Goto, H. Shintani, K. Ishizaka, T. Arima and Y. Tokura, Magnetic control of ferroelectric polarization, Nat. Mater. **426**, 55 (2003).

[23] N. Hur, S. Park, P. A. Sharma, J. S. Ahn, S. Guha and S.-W. Cheong, Electric polarization reversal and memory in a multiferroic material induced by magnetic fields, Nat. Mater. **429**, 392 (2004).

[24] Y. J. Choi, H. T. Yi, S. Lee, Q. Huang, V. Kiryukhin, and S.-W. Cheong, Ferroelectricity in an Ising chain magnet, Phys. Rev. Lett. **100**, 047601 (2008).

[25] A. Chatterjee, J. K. Dey, S. Majumdar, A.-C. Dippel, O. Gutowski, M. V. Zimmermann, and S. Giri, Tuning of multiferroic order with Co doping in CuCr$_2$O$_4$: Interplay between structure and orbital order, Phys. Rev. Mat. **3**, 104403 (2019).

[26] B. J. Kennedy, Q. Zhou, The role of orbital ordering in the tetragonal-to-cubic phase transition in CuCr$_2$O$_4$, J. Solid State Chem. **181**, 2227 (2008).

[27] Z. Ye, O. Crottaz, F. Vaudano, F. Kubel, P. Tissot, and H. Schmid, Single crystal growth, structure refinement, ferroelastic domains and phase transitions of the hausmannite CuCr$_2$O$_4$, Ferroelectrics **162**, 103 (1994).

[28] M. Tovar, R. Tobari, C. Welker, and F. Fleischer, Structural and magnetic properties of Cu–Ni–Cr spinel oxides, Phys. B: Condens. Matter **385-386**, 196 (2006).

[29] V. Kocsis, D. Varjas, K. Penc, A. Abouelsayed, C. A. Kuntscher, K. Ohgushi, Y. Tokura, and I. Kezsmark, Magnetoelasticity in ACr$_2$O$_4$ spinel oxides ($A =$ Mn, Fe, Co, Ni, and Cu), Phys. Rev. B **87**, 064416 (2013).

[30] M. C. Kemei, S. L. Moffitt, L. E. Darago, R. Seshadri, M. R. Suchomel, D. P. Shoemaker, K. Page, and J. Siewenie, Structural ground states of (A, A')Cr$_2$O$_4$ ($A =$ Mg, Zn; $A' =$ Co, Cu) spinel solid solutions: Spin-Jahn-Teller and Jahn-Teller effects, Phys. Rev. B **89**, 174410 (2014).

[31] S. Bordacs, D. Varjas, I. Kezsmarki, G. Mihaly, L. Baldassarre, A. Abouelsayed, C. A. Kuntscher, K. Ohgushi, and Y. Tokura, Magnetic-order-induced crystal symmetry lowering in ACr$_2$O$_4$ ferrimagnetic spinels, Phys. Rev. Lett. **103**, 077205 (2009).

[32] M. R. Suchomel, D. P. Shoemaker, and L. Ribaud, M. C. Kemei and R. Seshadri, Spin-induced symmetry breaking in orbitally ordered NiCr$_2$O$_4$ and CuCr$_2$O$_4$, Phys. Rev. B **86**, 054406 (2012).

[33] M. Reehuis, M. Tovar, D. M. Tobbens, P. Pattison, A. Hoser, and B. Lake, Competing Jahn-Teller distortions and ferrimagnetic ordering in the geometrically frustrated system Ni$_{1-x}$Cu$_x$Cr$_2$O$_4$, Phys. Rev. B **91**, 024407 (2015).

[34] K. Tomiyasu, S. Lee, H. Ishibashi, Y. Takahashi, T. Kawamata, Y. Koike, T. Nojima, S. Torii, and T. Kamiyama, Emergence of spin-orbit order in the spinel CuCr$_2$O$_4$, arXiv:1803.06447.

[35] A. Das, P. Pal, D. Ranaut, K. P. Islam, G. Bhattacharya, S. Mehta, A. Mondal, V. Adyam, K. Mukherjee, A. Das, and D. Choudhury, Origin of the long-range ferrimagnetic ordering in cubic Mn(Co)Cr$_2$O$_4$ spinels, Phys. Rev. B **107**, L100414 (2023).

[36] T. Roisnel and J. Rodriguez-Carvajal, WinPLOTR: A Windows tool for powder diffraction pattern analysis, Mater. Sci. Forum **378**, 118 (2000).

[37] A. A. Wagh, S. G. Bhat, V. K. Anusree, P.N. Santhosh, S. Elizabeth, P. S. Anil Kumar, Simple 4-segment thermal cycling pyroelectric measurement protocol for differentiating between ferroelectric and non-ferroelectric materials, Curr. Appl. Phys. **49**, 55 (2023).

[38] H. Nhalil, H. S. Nair, C. M. N. Kumar, A. M. Strydom, and S. Elizabeth, Ferromagnetism and the effect of free charge carriers on electric polarization in the double perovskite Y$_2$NiMnO$_6$, Phys. Rev. B **92**, 214426 (2015).

[39] V. K. Anusree, P. N. Lekshmi, S. G. Bhat, A. A. Wagh, G. Das, and P. N. Santhosh, Dielectric relaxation, magneto-dielectric coupling, and pyrocurrent anomaly in point defect controlled HoCrO$_3$, J. Appl. Phys. **127**, 194105 (2020).

[40] See Supplemental material at http://link.aps.org/supplemental/10.1103/PhysRevB.109.024104 for supporting structural, magnetization and pyrocurrent data. Rietveld refinement of the x-ray spectrum, EDX data analyses, analyses of frequency dependent dielectric data, DSC data are also included.

[41] C. G. Koops, On the dispersion of resistivity and dielectric constant of some semiconductors at audiofrequencies, Phys. Rev. **83**, 121 (1951).

[42] S. Mishra and Debraj Choudhury, Engineering DyCrO$_3$ ceramics toward room-temperature high-κ dielectric applications, J. Appl. Phys. **134**, 144101 (2023).

[43] C. Ang, Z. Yu, H. J. Youn, C. A. Randall, A. S. Bhalla, L. E. Cross, J. Nino, and M. Lanagan, Low-temperature dielectric relaxation in the pyrochlore $(Bi_{3/4}Zn_{1/2})_2(Zn_{1/4}Ta_{3/4})_7$ compound, Appl. Phys. Lett. **80**, 4807 (2002).

[44] C. Ang, Z. Yu, and L. E. Cross, Oxygen-vacancy-related low-frequency dielectric relaxation and electrical conduction in Bi:SrTiO$_3$, Phys. Rev. B **62**, 228 (2000).

[45] L. Rossi, D. Brüning, H. Ueda, Y. Skourski, T. Lorenz, and B. Bryant, Magnetoelectric coupling in a frustrated spinel studied using high-field scanning probe microscopy, Appl. Phys. Lett. **116**, 262901 (2020).

[46] Ch. Kant, J. Deisenhofer, T. Rudolf, F. Mayr, F. Schrettle, A. Loidl, V. Gnezdilov, D. Wulferding, P. Lemmens, and V. Tsurkan, Optical phonons, spin correlations, and spin-phonon coupling in the frustrated pyrochlore magnets CdCr$_2$O$_4$ and ZnCr$_2$O$_4$, Phys. Rev. B **80**, 214417 (2009).

[47] J.-H. Chung, Y. S. Song, S. Park, H. Ueda, Y. Ueda, and S.-H. Lee, Incommensurate spin spiral of the geometrically-frustrated antiferromagnet CdCr$_2$O$_4$, J. Korean Phys. Soc. **62**, 1900 (2013).

[48] A. Das, D. Ranaut, P. Pal, R. Pal, S. Moulick, M. Das, D. Topwal, P. Mandal, A. N. Pal, K. Mukherjee, and D. Choudhury, Tuning of magnetic frustration and emergence of a magnetostructural transition in $Mn_{1-x}Cd_xCr_2O_4$, Phys. Rev. B **108**, 064426 (2023).

[49] T. N. M. Ngo, U. Adem, and T. T. M. Palstra, The origin of thermally stimulated depolarization currents in multiferroic $CuCrO_2$, Appl. Phys. Lett. **106**, 152904 (2015).

[50] A. Pal, C. Dhana Sekhar, A. Venimadhav, W. Prellier and P. Murugavel, Investigations on the defect dipole induced pyroelectric current in multiferroic $GdMnO_3$ system, J. Appl. Phys. **123**, 014102 (2018).

[51] A. Almeida, T. M. Correia, M. R. Chaves, P. M. Vilarinho, A. L. Kholkin, and A. M. Costa, Study of polar relaxation processes in $Sr_{1-1.5x}La_xTiO_3$ ceramics by using field-induced thermally stimulated currents, J. Eur. Ceram. Soc. **27**, 3701 (2007).